COBEM 2023 27TH INTERNATIONAL CONGRESS OF MECHANICAL ENGENEERING

ABCM Brazilian Society of Mechanical Sciences and Engineering
27th ABCM International Congress of Mechanical Engineering
December 04-08, 2023, Florianópolis-SC, Brazil

DYNAMIC ANALYSIS OF RAILWAYS TRACKS USING THE SPECTRAL ELEMENT METHOD

Pedro Augusto Beck[1]
Geder Gabriel Louback Cunha[1]
pedro.ag.beck@gmail.com gedergabriel@gmail.com
Douglas D. Bueno[2]
douglas.bueno@unesp.br
Rodrigo Borges Santos[1]
rodrigobsantos@ufgd.edu.br
[1]Federal University of Grande Dourados (UFGD), Faculty of Engineering, Department of Mechanical Engineering, Dourados, MS, Brazil.
[2]São Paulo State University (UNESP), School of Engineering, Department of Mathematics, Ilha Solteira, SP, Brazil.

Abstract. *Rail transport is an excellent option to large scale transportation because it usually can transport very high loads, mainly raw materials and passengers. New challenges and opportunities are offered to the classical railway engineering and requires a better understanding of the railway track dynamics for establishing different engineering applications. A structure healthy monitoring (SHM) process focused on damage detection along the railway track usually is a challenge task due to the length of this type of structure. In this sense, a major step for introducing a SHM-process is to create a representative dynamic model in the frequency domain, with accuracy for high frequencies, mainly for the model-based SHM methodologies. In this context, the main goal of this work is to introduce a dynamic model for railway tracks based on the Spectral Element Method. This type of approach involves a relatively low computational cost once its solution is closer to the analytical solution. The dynamic effects of the rail, rail-pads, sleeper, the ballast stiffness and damping are included to evaluate the influence of each one on the system response. Numerical results are presented to demonstrate the feasibility of the proposed approach to describe the dynamics of railway tracks.*

Keywords: *Railway, Dynamics, Damage Index, SHM, Spectral Element.*

1. INTRODUCTION

Goods and passenger transportation systems are very important for the development of a region, and they contribute for turning its economy around. In Brazil, the predominance of roads over rail tracks and waterways is evident due to the discrepancy of kilometers of road network implemented in relation to the other transport networks. Roads have both positive and negative aspects in relation to other types of transportation. The main positive ones are a typical route flexibility and speed of transport, whereas the negative ones are high maintenance costs and low cargo transport capacity. Rail systems, on the other hand, which began to be implemented in Brazil around the nineteenth century, have as their main advantages the great transport capacity, the possibility of continental dimensions and relatively low maintenance costs, as opposed to low transport speed and no route flexibility (fixed routes). It is an excellent way of transporting goods and passengers, and it has been undergoing a growing development of new technologies, thus opening several fields of study involving this means of transport.

One of the fields of study and development of technologies is the field of structural health analysis, known as Structural Health Monitoring (SHM), presented in detail in Farrar and Worden (2007) SHM is commonly, characterized by the use of tools and strategies, applied in an organized way, aimed at detecting damage to structural integrity. The main objective this topic is to quickly and accurately characterize and detect flaws in structures and it's used in services where the area swept area is large, such as the integrity of the structure of a skyscraper or the search for cracks in the structure of an airplane, for example. SHM technique is an combine numerical methods to build mathematical models to be computationally simulated and compared with experimental results. These models can be classified through two different domains: time and frequency (Lee, 2009). The frequency-domain based methods, an use the Spectral Element method(SEM) which presents certain advantages over other ones, such as the high accuracy of the responses in the frequency domain, use of a reduced number of elements to represent the behavior of a structure, relatively low computational cost and no the capacity perform the analysis involving shear.

SHM studies on rails can employ several different methodologies. Imdad *et al.* (2015) implemented a low-cost acquisition system to obtain, experimentally, a database of responses covering healthy and unhealthy conditions to detect damages. Ryue *et al.* (2008) employed the Wavenumber Finite Element Method, to investigate how a wave moves on a rail, focused on the interference of waves with low frequencies and with high frequencies. Gonsalez-Bueno (2019) studied the effects of wave propagation in beams involving symmetrical and asymmetrical damages, evaluate longitudinal

and flexural waves. El Mouedded *et al.* (2022) use a numerical methodology involving the Finite Element Method to represent a rail system composed of a rail, rail-pad, sleeper and ballast, they study the structural fatigue caused by external disturbances, focused on developing improved railway tracks. Thompson (1993) employs FEM(Finite element method) to evaluate the frequency range from 100 to 500 Hz, and show that there is significant deformation of the rail cross section at higher frequencies.

This paper aims to develop a using dynamic model to describe the basically rail, rail-pad, sleeper and ballast of one side of a railway track using of the Spectral Elements Method. Numerical simulations are carried out to investigate the dynamic responses for rails considering different damage locations (rail-pad, ballast and rail). The results demonstrate that the employed approach provide interesting information for damage detection in rail ways track.

2. RAILWAY MODEL

A schematic representation of a train line is shown in Fig. 1 (a). The system is composed of two rails, rail- pads, ballast, and a sleeper. The rails are the main structural components and they are subjected to the main stresses transmitted by the locomotives and they serve as guides for the train motion. The rail-pads distribute loads between rails and ties contribute and for reducing vibrations. The sleepers are responsible for redistributing the loads to the ballast, and contribute to keep the distance between rails and track stability. The ballast is the foundation for the railroad's construction, responsible for evenly distributing loads, water drainage, and rail stabilization.

A dynamic model considered to represent a half track of the rail an it is illustrated in Fig. 1 (b). Note that the model of a single part of the rail (i.e. cell) is composed of a beam element and a mass-spring-damper system to represent the dynamics of the rail-pad, sleeper and ballast. Longitudinal displacements are neglected and therefore only vertical (y) and rotational (θ) displacements are considered. The rail characteristics are defined by the moment of inertia I_z, cross-sectional area S_r, Young's modulus E , mass density ρ and length of each beam element l. The related rail-pad and ballast pairings are defined by the stiffness coefficients k_p, k_b and the damping coefficients c_p and c_b, respectively. The sleepers are considered as a rigid body and the mass of half a sleeper is given by m_s. The rail profile is shown in Fig. 1 (c) and, its characteristics can be obtained from the VALE technical manual UIC 60 rail model (VALE, 2009).

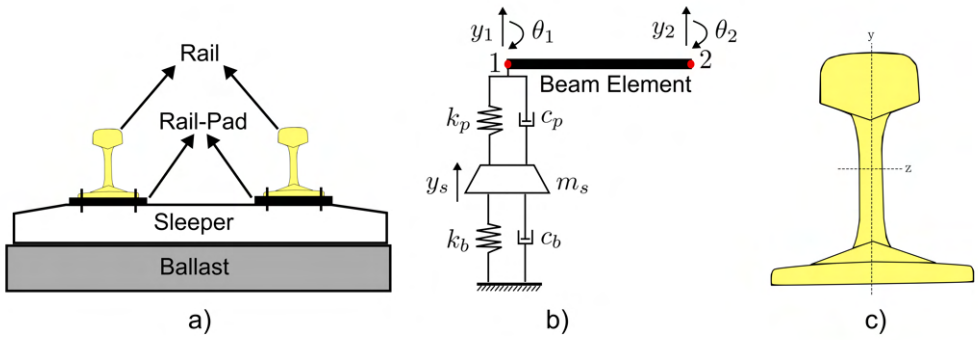

Figure 1. a) Schematic representation of a train line, b) Unit cell and b) Rail cross-section.

The model for a complete train line considering n cells is shown in Fig.2. Note that at the end of the line it is necessary to include a mass-spring-damper system to complete the model.

The modeling of the rail is performed using Spectral Element Method considering the Euler-Bernoulli type beam, and its formulation is shown in detail in Lee (2009). The equation of motion representing the dynamics of the beam element is given by $\boldsymbol{D}\,\boldsymbol{u}=\boldsymbol{F}$, where $\boldsymbol{u}$ is the vector of nodal displacements given by $\boldsymbol{u}=\{y_1\ \theta_1\ y_2\ \theta_2\}$, $\boldsymbol{F}$ is the vector of the nodal transverse forces (V) and moments (M) given by $\boldsymbol{F}=\{V_1\ M_1\ V_2\ M_2\}$ and $\boldsymbol{D}$ is the dynamic stiffness matrix of the beam element of the unit cell, given by Eq. 1 and is represented in Fig. 1 (b), where ω is the frequency in rad/s.

$$\mathbf{D}(\omega) = \begin{bmatrix} D_{11} & D_{12} & D_{13} & D_{14} \\ D_{12} & D_{22} & D_{23} & D_{24} \\ D_{13} & D_{23} & D_{33} & D_{34} \\ D_{14} & D_{24} & D_{34} & D_{44} \end{bmatrix} \tag{1}$$

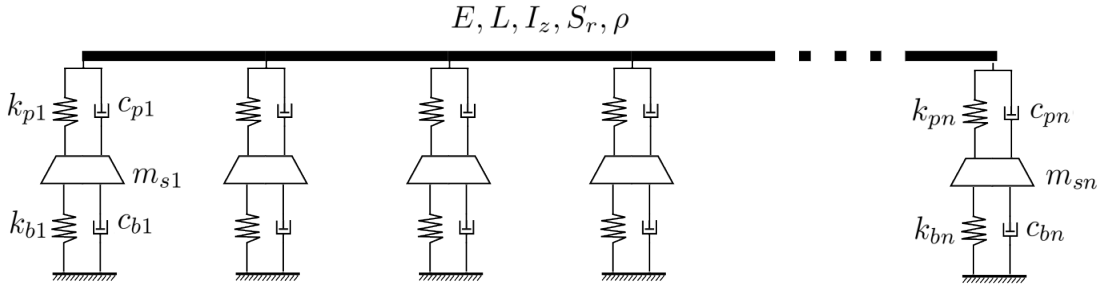

Figure 2. Simplified model of a train track containing n-cells.

Where the terms of the matrix elements are given by the following equations.

$$
\begin{aligned}
&D_{11} = D_{33} = \tfrac{EI_z}{l^3}\Delta_b l_b^3(cos(l_b)sinh(l_b) + sin(l_b)cosh(l_b))\\
&D_{22} = D_{44} = \tfrac{EI_z}{l^3}\Delta_b l_b^3 k_f^{-2}(-cos(l_b)sinh(l_b) + sin(l_b)cosh(l_b))\\
&D_{12} = -D_{34} = \tfrac{EI_z}{l^3}\Delta_b l_b^3 k_f^{-1}(sin(l_b)sinh(l_b))\\
&D_{13} = -\tfrac{EI_z}{l^3}\Delta_b l_b^3(sin(l_b) + sinh(l_b))\\
&D_{14} = -D_{23} = \tfrac{EI_z}{l^3}\Delta_b l_b^3 k_f^{-1}(-cos(l_b)cosh(l_b))\\
&D_{24} = \tfrac{EI_z}{l^3}\Delta_b l_b^3 k_f^{-2}(-sin(l_b)sinh(l_b))\\
&k_f = \sqrt{\omega}\left(\tfrac{\rho S_r}{EI_z}\right)^{\frac{1}{4}}\\
&l_b = k_f l\\
&\Delta_b = \tfrac{1}{1-cos(l_b)cosh(l_b)}
\end{aligned}
\tag{2}
$$

The dynamic stiffness matrix of the mass-spring-damper system of the unit cell shown in Fig. 1 (b) is given by Eq. 3.

$$
\mathbf{D}_s = K + i\omega C - \omega^2 M = \begin{bmatrix} D_{s11} & D_{s12} \\ D_{s21} & D_{s22} \end{bmatrix} \tag{3}
$$

Where the stiffness K, damping C, and mass M matrices are given by the Eq. 4.

$$
\mathbf{K} = \begin{bmatrix} k_p & -k_p \\ -k_p & k_b + k_p \end{bmatrix};\ \mathbf{C} = \begin{bmatrix} c_p & -c_p \\ -c_p & c_b + c_p \end{bmatrix};\ \mathbf{M} = \begin{bmatrix} 0 & 0 \\ 0 & m_s \end{bmatrix} \tag{4}
$$

The dynamic stiffness matrix of a single cell D_{cell}, shown in Fig. 1 (b), can then be obtained by coupling the corresponding degrees of freedom of the mass-spring-damper system with the beam element. Then Eq. 5 is obtained, and the global dynamic stiffness matrix D_g of the system with n (showed in Fig. 2) cells can be obtained by assembling the elementary matrices of each cell using a strategy similar to that employed when using the conventional FEM. The results are presented in a non-dimensional frequency given by $\Omega = \frac{k_f l}{\pi}$ where k_f is the flexural wave number. The normalization of the dimension frequency is performed with respect to the length of each beam element l (i.e., the cell length). The value of the non-dimensional frequency can also be given by $\Omega = \frac{2l}{\lambda}$, where λ is the flexural wavelength.

$$
\mathbf{D}_{cell} = \begin{bmatrix}
D_{11} + D_{s11} & D_{12} & D_{s12} & D_{13} & D_{14} \\
D_{12} & D_{22} & 0 & D_{23} & D_{24} \\
D_{s21} & 0 & D_{s22} & 0 & 0 \\
D_{13} & D_{23} & 0 & D_{33} & D_{34} \\
D_{14} & D_{24} & 0 & D_{34} & D_{44}
\end{bmatrix} \tag{5}
$$

3. RESULTS AND DISCUSSIONS

In this section three different structural damage conditions are investigated. The analyses are carried out considering a rail structure composed of 5 elements (6 nodes) and each element with a length of 0.6 m. In the first and second case of damage is considered loss of stiffness and damping in the rail-pad and ballast, in the third case is considered damage to the rail, where in this case the damage is of the geometric type represented by changes in the moment of inertia I_z. Table. 1 shows the three damage cases studied. Note that the analysis starts from a totally healthy structure (baseline), i.e. 0% damage, up to a structure with 100% damage. Table. 2 shows the values used for the parameters of the mass-spring-damper system and the rail obtained in El Moueddeb *et al.* (2022) and VALE (2009).

Table 1. Damage conditions for the three cases studied.

Damage	Pad		Ballast		Rail
%	$k_p\ [N/m]$	$c_p\ [Ns/m]$	$k_b\ [N/m]$	$c_b\ [Ns/m]$	$I_z[m^4]$
0	$350 \cdot 10^6$	$50 \cdot 10^6$	$50 \cdot 10^6$	$100 \cdot 10^6$	$3.0383 \cdot 10^{-5}$
5	$332.5 \cdot 10^6$	$47.5 \cdot 10^6$	$47.5 \cdot 10^6$	$95 \cdot 10^6$	$2.8864 \cdot 10^{-5}$
15	$297.5 \cdot 10^6$	$42.5 \cdot 10^6$	$42.5 \cdot 10^6$	$85 \cdot 10^6$	$2.5825 \cdot 10^{-5}$
85	$52.5 \cdot 10^6$	$7.5 \cdot 10^6$	$7.5 \cdot 10^6$	$15 \cdot 10^6$	$0.4557 \cdot 10^{-5}$
95	$17.5 \cdot 10^6$	$2.5 \cdot 10^6$	$2.5 \cdot 10^6$	$5 \cdot 10^6$	$0.1519 \cdot 10^{-5}$
99	-	-	-	-	$0.003 \cdot 10^{-5}$
100	0	0	0	0	-

Table 2. Values for the parameters of the mass-spring-damper system and the rail.

Rail				
$E[Pa]$	$\rho[kg/m^3]$	$S_r[m^2]$	$I_z[m^4]$	$l[m]$
$210 \cdot 10^9$	7850	$7.67 \cdot 10^{-3}$	$3.0383 \cdot 10^{-5}$	0.6
Mass-spring-damper system				
$k_p[N/m]$	$k_b[N/m]$	$c_p[Ns/m]$	$c_b[Ns/m]$	$m_s[kg]$
$350 \cdot 10^6$	$50 \cdot 10^6$	$50 \cdot 10^6$	$100 \cdot 10^6$	162

3.1 Damaged: ballast

The results of the damage applied to the Ballast are shown in Fig. 3, where the percentage of damage to the structure are 0%, 5%, 15%, 85%, 95% and 100%. They are applied in damper and spring located at the third node. The result show relevant difference from the Baseline if 100% damage are considered and for the other damages level the change is almost imperceptible. Fig. 4 (a) and (b) show the zoomed view for the frequency range from 1 to 1.5 and 2 to 2.5 respectively. Fig. 4 (a) show a slight shift to right of the frequencies for 100% damage, and a slight difference in the amplitude for the 100%, 95%, and 85% levels in the 1.45 frequency range, in comparison with to the baseline condition.

A damage index (σ) is defined as the ration between the H_2 norms of the FRF of the structure with damage and without damage (baseline), i.e., $\sigma = \frac{|H_2^d|}{|H_2^b|}$. The H_2 norm represents the area under the curve of the FRF. Fig. 5 (a) and Fig. 5 (b) show the damage indexes (following the same color pattern as Fig. 3) for the frequency range of 1 to 1.5 and 2 to 2.5, respectively. Note for both frequency ranges, for the damage levels of 5% and 15%, there is almost no variation of σ, but for 100%, 95%, 85% the variation becomes significant. So, the system is little sensitive to damage when the values of stiffness and damping are close to the baseline value (little damage) and the sensitivity increases as the damage increases.

Note that in the case of 100% damage, the FRF shifted upwards (see Fig. 3 and Fig. 4) in relation to the baseline condition, which resulted in a higher σ value for this condition (see Fig. 5). This is an important characteristic for monitoring the integrity of the structure, as it indicates the condition in which the ballast is decoupled from the rail-pad and rail.

Figure 6 shows the damage index for different damage positions (i.e., different nodes), and this is normalized with respect to its maximum value. Note that the largest index are at the input and output positions of the structure, that is, at the node where the structure is excited and at the node where the response is measured. It is also possible to note, a characteristic behavior of the FRF (reciprocity), since, the damage index for positions 1 and 6, 2 and 5 , 3 and 4 are identical to each other. This is an important characteristic to locate the damage.

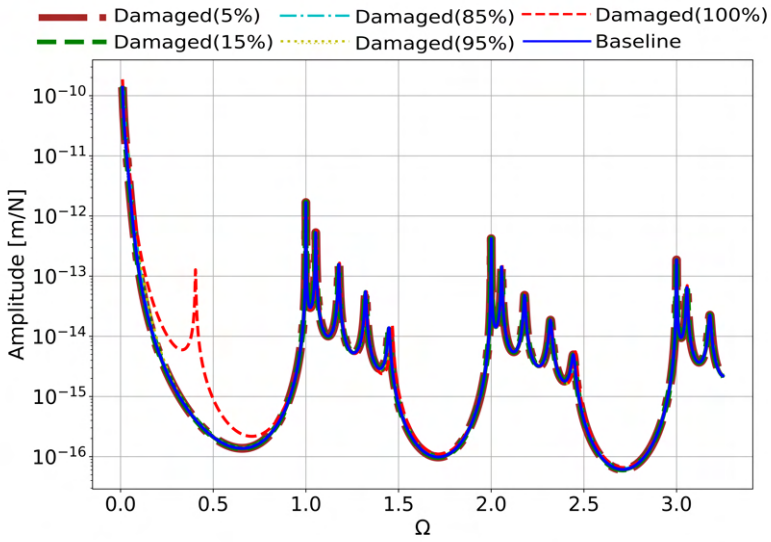

Figure 3. Results obtained in terms of Frequency Response Functions (FRF) for the ballast, for different damage percentage to the third node.

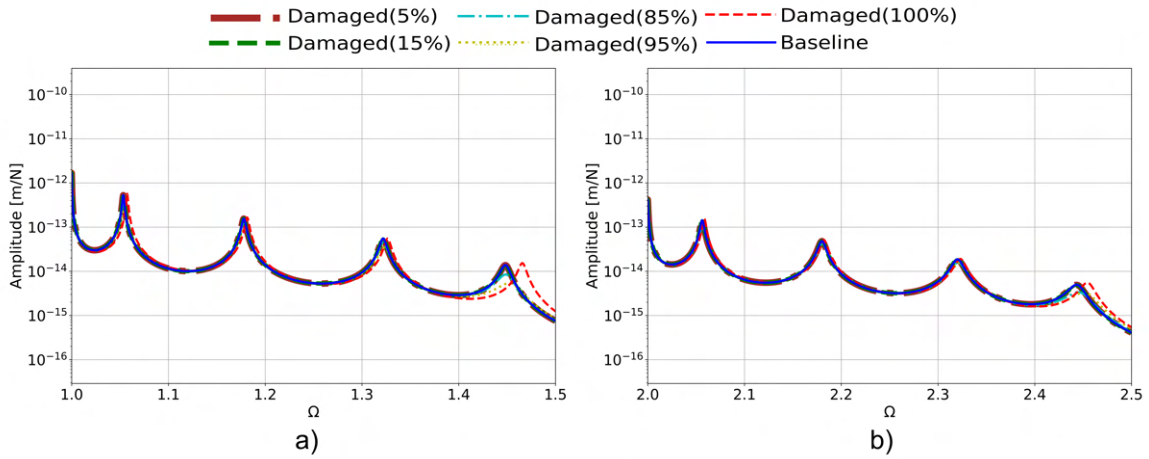

Figure 4. Results obtained in terms of FRFs for the ballast, for different damage percentage to the third node: a) $1 < \Omega < 1.5$ and b) $2 < \Omega < 2.5$.

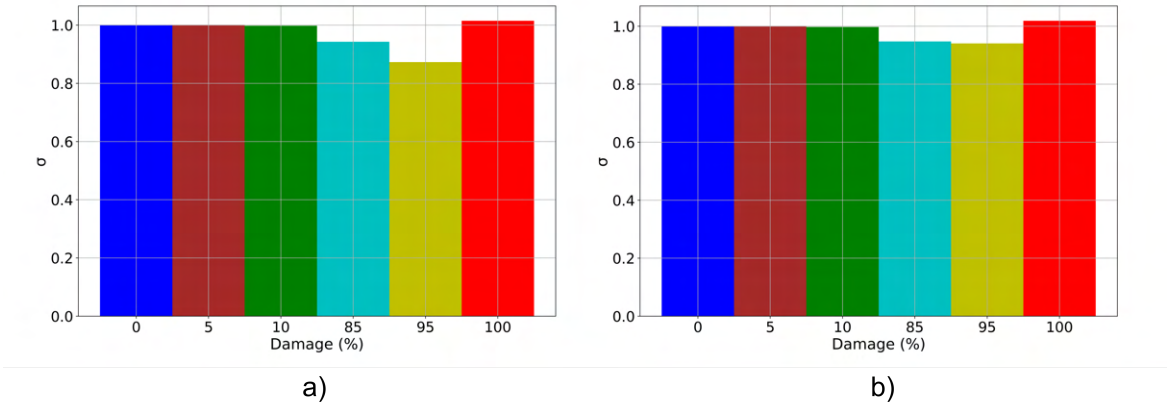

Figure 5. Damage index (σ) for the ballast, for different damage percentage to the third node: a) $1 < \Omega < 1.5$ and b) $2 < \Omega < 2.5$.

3.2 Damaged: rail-pad

The results of the damage applied to the Rail-Pad are shown in Fig. 7, where in the same way as for Ballast, the damage to the structure varies in the same ranges. In general, the FRF response does not show large differences for

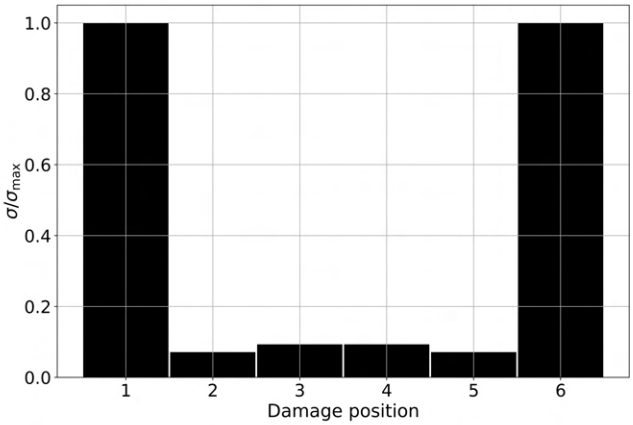

Figure 6. Normalized damage index (σ/σ_{max}) for the ballast (100% damaged), for different damage positions ($\sigma_{max} = 12.87$).

different damage to the Rail-Pad, with the exception of the 100% damage case, as for this case the system shows more significant differences.

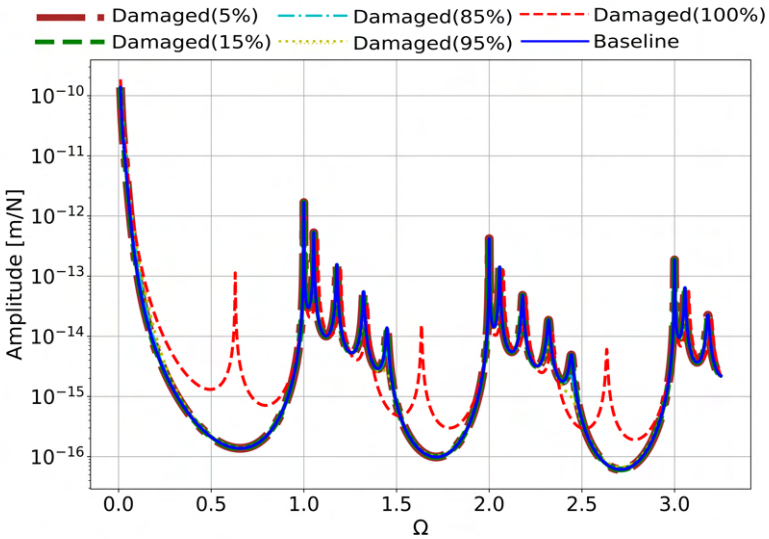

Figure 7. Results obtained in terms of FRFs for the rail-pad, for different damage percentages to the third node .

A magnification was applied to the FRF of Fig. 7, in the same way as in Ballast, with the Ω intervals between 1 to 1.5 and 2 to 2.5, shown in Fig. 8 (a) e (b). In this case, the 100, 95 and 85% damages show more obvious amplitudes, with the variation much more significant for the 100% case, there being not only amplitude variation but also the displacement of these frequencies to the right.

For damage index calculated at Ω intervals between 1 to 1.5; 2 to 2.5, the results are shown in Fig. 9 (a) e (b). In this, it is noticeable that as the damage increases, σ decreases, except for the case of 100%, where it increased compared to the previous damage. Another behavior is that for little damage to the structure (in the cases of 5 and 15%) there is little variation of the σ value between these cases, as well as found in the ballast. So, it is also clear that for large damage, large variations are observed, so consequently large variation of the FRF.

Note that in the case of 100% damage, the FRF shifted upwards (see Fig. 7 and Fig. 8) in relation to the baseline condition, which resulted in a higher σ value for this condition (see Fig. 9). This is an important characteristic for monitoring the integrity of the structure, as it indicates the condition in which the rail-pad is decoupled from the rail.

Figure 10 shows the damage index for different damage positions obtined for the rail-pad. Just as for the ballast, you can observe largest index are at the input and output positions of the structure and also is present the characteristic behavior of the reciprocity.

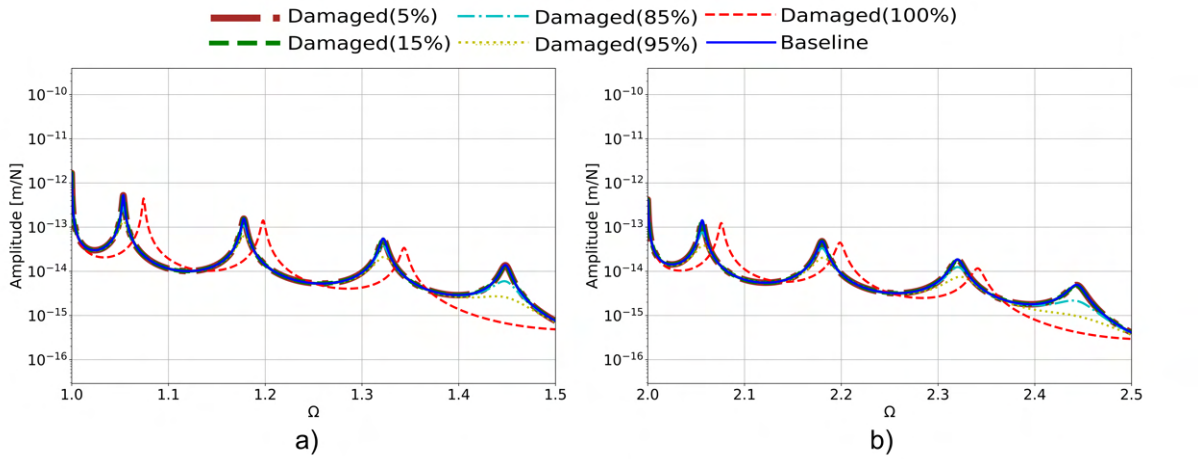

Figure 8. Results obtained in terms of FRFs for the rail-pad, for different damage percentages to the third node: a) $1 < \Omega < 1.5$ and b) $2 < \Omega < 2.5$.

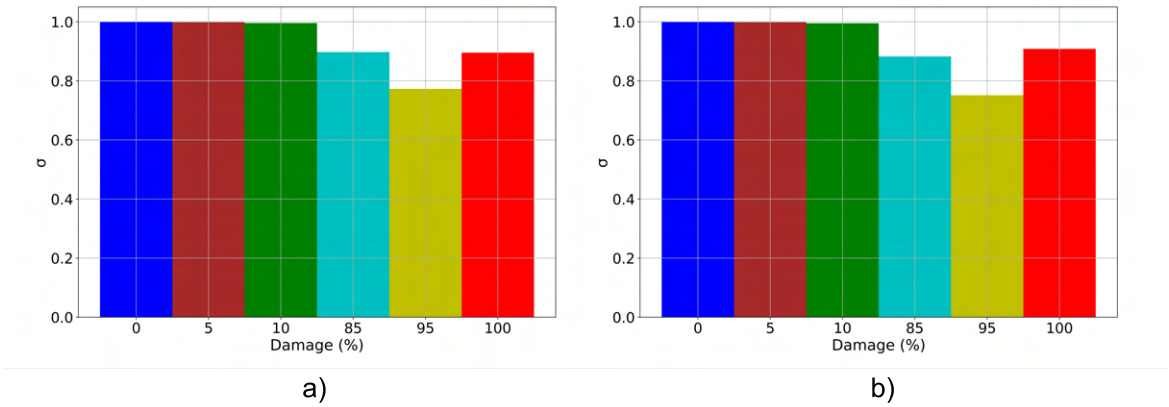

Figure 9. Damage index (σ) for the rail-pad, for different damage percentages to the third node: a) $1 < \Omega < 1.5$ and b) $2 < \Omega < 2.5$.

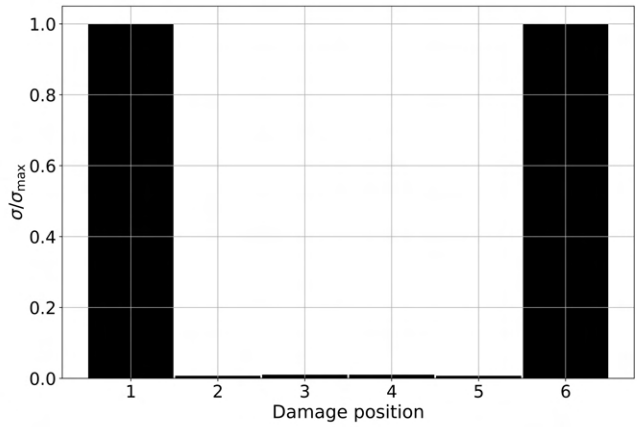

Figure 10. Normalized damage index (σ/σ_{max}) for the rail-pad (100% damaged), for different damage positions ($\sigma_{max} = 119.74$).

3.3 Damaged: rail

Following the same methodology, the damage responses applied to the rail are shown in Fig. 11. For this case, a greater difference in results were observed, for which all curves stood out more clearly.

The frequency ranges analyzed are the same as those for ballast and rail-pad, 1 to 1.5 and 2 to 2.5, as shown in

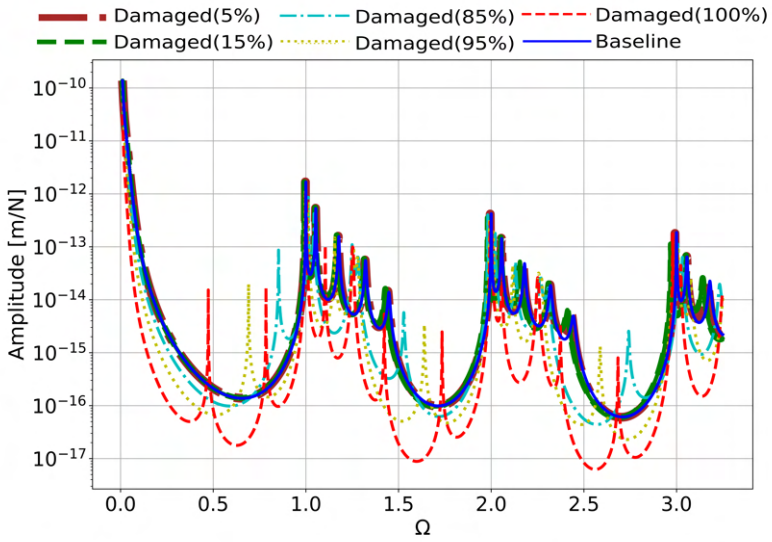

Figure 11. Results obtained in terms of FRFs for the rail, for different damage percentages to the third beam element.

Fig. 12(a) and (b). It is noticeable that each percentage of damage corresponded to a different curve, from light damage (5%), to critical damage (99%). Thus indicating that even for light damage to the rail the system response differently, unlike ballast and rail-pad which for light damage there was little variation. This results are evident in terms of damage index as shows the Fig. 13(a) and (b). Observe that the value of σ varies considerably from one case to the other for all percentages of damage and and these values only decrease with increasing damage.

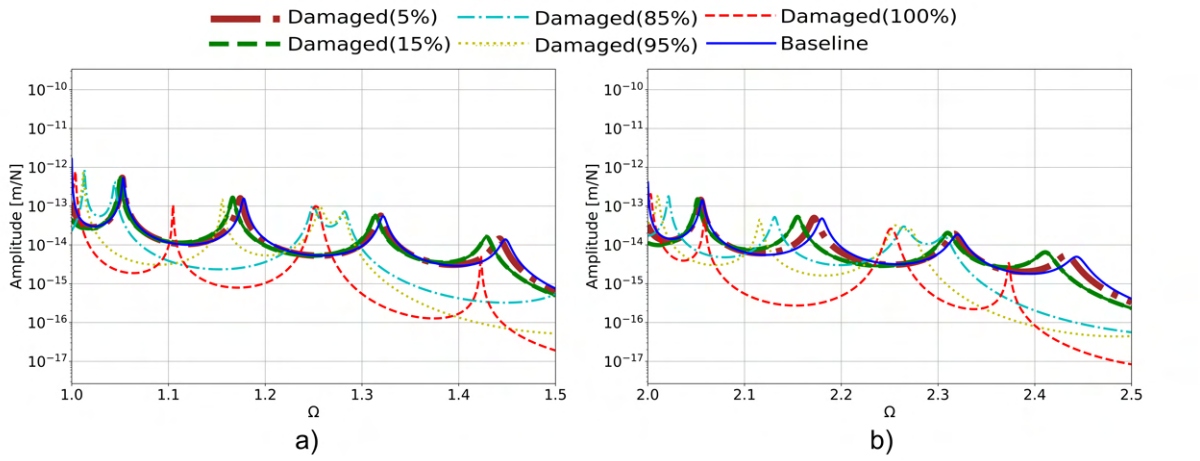

Figure 12. Results obtained in terms of FRFs for the rail, for different damage percentages to the third beam element: a) $1 < \Omega < 1.5$ and b) $2 < \Omega < 2.5$.

Note that in the case of 99% damage, the FRF shifted downwards (Fig. 12) in relation to the baseline condition, contrary to what happened for the ballast and rail-pad, which resulted in a lower σ value for this condition (Fig. 13). This is an important characteristic for monitoring the integrity of the structure, as it indicates the condition in which the rail is almost completely broken.

Figure 14 shows the damage index for the rail considering different damage positions. In contrast to the damage cases for the ballast and rail-pad, the results show smaller index values input and output positions of the structure and the central position (node 3) has the highest damage index. And, the characteristic of reciprocity is also observed for the results.

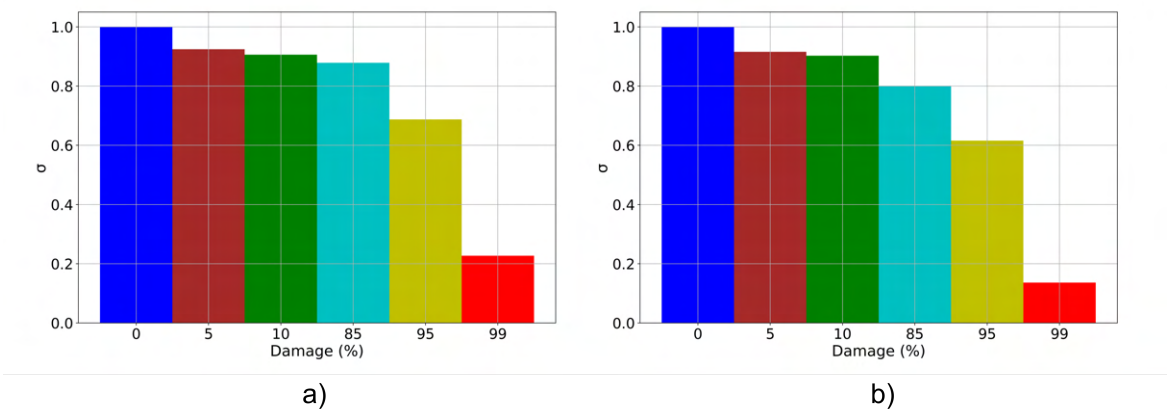

Figure 13. Damage index (σ) for the rail, for different damage percentages to the third beam element: a) $1 < \Omega < 1.5$ and b) $2 < \Omega < 2.5$.

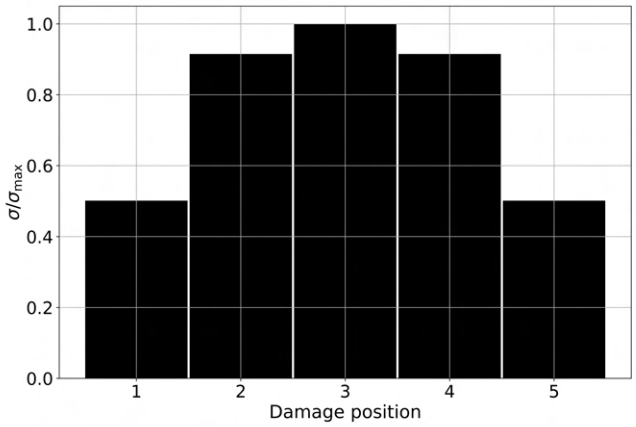

Figure 14. Normalized damage index (σ/σ_{max}) for the rail (99% damaged), for different damage positions (σ_{max}=0.12).

4. CONCLUSION

In this paper, a simplified dynamic model for half railway tracks based on the Spectral Element Method is presented for understanding the dynamics of the track when its components, rail, rail-pad and ballast are subjected to a damage condition. Thus, the influence of each of them on the system response is evaluated. When ballast or rail-pad damage is considered, low sensitivity in damage detection is observed, since for small percentages of damage, no significant changes are observed in the FRF curves relative to the baseline condition, which can also be seen in the damage indexes. And, when considering different positions for damage, reciprocal characteristics of the results can be noted. On the other hand, when damage was considered on the rail, a better sensitivity in damage detection was observed. Therefore, in this case, the present approach can be an important tool for SHM analyses.

5. ACKNOWLEDGMENTS

The third and fourth authors thank to São Paulo Research Foundation (FAPESP), Brazil, grant number 2022/10174-5.

6. REFERENCES

El Moueddeb, M., Louf, F., Boucard, P.A., Dadié, F., Saussine, G. and Sorrentino, D., 2022. "An efficient numerical model to predict the mechanical response of a railway track in the low-frequency range". *Vibration*, Vol. 5, No. 2, pp. 326–343.

Farrar, C.R. and Worden, K., 2007. "An introduction to structural health monitoring". *Philosophical Transactions of the Royal Society A: Mathematical, Physical and Engineering Sciences*, Vol. 365, No. 1851, pp. 303–315.

Gonsalez-Bueno, C.G., 2019. "An investigation into the way in which longitudinal and flexural waves interact with corrosion-like damage".

Imdad, F., Niaz, M.T. and Kim, H.S., 2015. "Railway track structural health monitoring system". In *2015 15th International Conference on Control, Automation and Systems (ICCAS)*. IEEE, pp. 769–772.

Lee, U., 2009. *Spectral element method in structural dynamics*. John Wiley & Sons.

Ryue, J., Thompson, D.J., White, P.R. and Thompson, D., 2008. "Wave propagation in railway tracks at high frequencies". In *Noise and Vibration Mitigation for Rail Transportation Systems: Proceedings of the 9th International Workshop on Railway Noise, Munich, Germany, 4-8 September 2007*. Springer, pp. 440–446.

Thompson, D., 1993. "Wheel-rail noise generation, part iii: rail vibration". *Journal of sound and vibration*, Vol. 161, No. 3, pp. 421–446.

VALE, 2009. "Manual técnico da via permanente".

7. RESPONSIBILIRY NOTICE

The authors are solely responsible for the printed material included in this paper.